CCS Chemistry

RESEARCH ARTICLE

Received: Mar. 16, 2020 | Accepted: May 25, 2020 | Published: June 30, 2020

Structural Insight into the Substrate Gating Mechanism by *Staphylococcus aureus* Aldehyde Dehydrogenase

Xuan Tao[1†], Zhemin Zhang[1†], Xiao Zhang[1], Hongyan Li[2], Hongzhe Sun[2*], Zong-Wan Mao[1] & Wei Xia[1*]

[1]*MOE Key Laboratory of Bioinorganic and Synthetic Chemistry, School of Chemistry, Sun Yat-sen University, Guangzhou, 510275,* [2]*Department of Chemistry, The University of Hong Kong, Pokfulam Road, Hong Kong.*

**Corresponding authors: xiawei5@mail.sysu.edu.cn; hsun@hku.hk;* [†]X. Tao and Z. Zhang contributed equally to this work.

Cite this: *CCS Chem.* **2020**, *2*, 946–954

Staphylococcus aureus **produces staphyloxanthin, a C_{30} carotenoid with golden color, as an antioxidant to promote bacterial resistance to reactive oxygen species. The biosynthesis pathway of staphyloxanthin involves a series of catalytic enzymes. Aldehyde dehydrogenase (AldH) is a dehydrogenase recently identified to convert 4,4'-diaponeurosporenaldehyde into 4,4'-diaponeurosporenoic acid during staphyloxanthin biosynthesis. Here, we present the crystallographic structures of apo- and holo-forms of *S. aureus* AldH. The dimeric enzyme contains a unique C-terminal helix, which resembles a "gatekeeper" helix found in human membrane-bound fatty aldehyde dehydrogenase (FALDH). Particularly, the helix adopts "open" and "closed" conformations in apo- and holo-AldH, respectively, to control the access of the substrate tunnel. Mutagenesis in combination with *in vitro* and *in vivo* activity assays identifies several residues essential for *S. aureus* AldH substrate recognition and enzyme catalytic turnover. Our results provide insights into substrate recognition of *S. aureus* AldH toward polyunsaturated long-chain aldehydes at atomic resolution.**

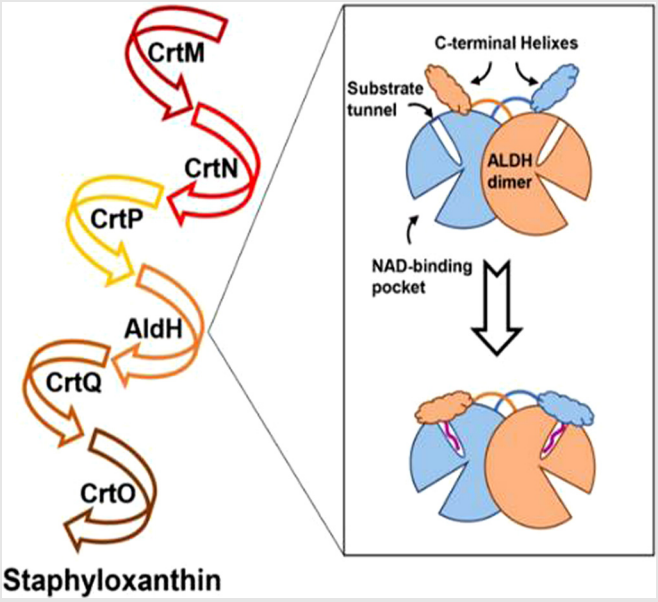

Keywords: ***Staphylococcus aureus*****, virulence factor, substrate recognition, aldehyde dehydrogenase, protein structure**

DOI: 10.31635/ccschem.020.202000219
Citation: *CCS Chem.* **2020**, 2, 946–954
Citation denotes calendar and volume year of first online publication.
Issue Assignment: Volume 2 (2020), Issue 5

Introduction

Staphylococcus aureus is a widespread human pathogen that can cause a series of infectious disorders ranging from relatively benign to life-threatening diseases.[1] Due to the abuse of antibiotics, the emergence of drug-resistant *S. aureus*, such as methicillin-resistant (MRSA) and vancomycin-resistant *S. aureus* strains (VRSA), have become serious global public health threats.[2] Meanwhile, there has been a lack of productivity in the discovery of new antibiotics, creating an urgent need for the development of novel anti-infective therapies. Via neutralization of virulence factors to render pathogen bacteria susceptible to human immune system clearance, antivirulence therapy has become an alternative approach to combat bacterial infections.[3,4] Such a strategy poses less selective pressure, which may reduce the emergence of drug resistance.[5]

More than 90% of *S. aureus* clinical isolates generate a golden pigment staphyloxanthin, a C_{30} carotenoid virulence factor.[6] Previous studies have demonstrated that staphyloxanthin functions as an antioxidant to protect the bacteria from oxidative stress.[7] Bacteria that lack the pigment can grow normally but are susceptible to human neutrophil killing.[8] A recent study demonstrates that staphyloxanthin also condenses in the functional membrane micro-domain of *S. aureus* to maintain bacterial membrane integrity.[9,10] Given the essential role of staphyloxanthin, blocking its biosynthetic pathway is a potential antivirulence strategy to combat *S. aureus* infection.[11–13] The genes involved in staphyloxanthin biosynthesis were initially identified to be in a *crtOPQMN* operon, which can encode five enzymes to catalyze the stepwise conversion of two farnesyl diphosphate molecules into staphyloxanthin.[14,15] Recently, the sixth pathway enzyme, *S. aureus* 4,4'-diaponeurosporen-aldehyde dehydrogenase (*Sa*AldH), was identified to catalyze the oxidation reaction of 4,4'-diaponeurosporen-4-al into 4,4'-diaponeurosporenoic acid. When *Sa*AldH is coexpressed with CrtOPQMN in an *Escherichia coli* host, staphloxanthin- and staphyloxanthin-like compounds can be produced (Figure 1).[16]

*Sa*AldH belongs to the superfamily of aldehyde dehydrogenases (ALDHs), which are homo-oligomeric enzymes catalyzing the $NAD(P)^+$-dependent oxidation of aldehydes to carboxylic acids.[17] ALDHs process a diverse array of substrates, ranging from small acetaldehyde to long fatty aldehyde.[18–20] Therefore, ALDH family enzymes usually have substrate binding pockets with different sizes and shapes to accommodate their specific substrates. For example, sheep liver ALDH1 substrate tunnel is more open than its counterpart in ALDH2. Therefore, ALDH1 prefers larger, bulkier retinal as a substrate, whereas ALDH2 prefers acetaldehyde.[18,21,22] Notably, the substrate of *Sa*AldH, 4,4'-diaponeurosporen-4-al, is an extremely long polyunsaturated aldehyde (C_{30}). Therefore, a key unresolved question in staphyloxanthin biosynthesis is how *Sa*AldH recognizes 4,4'-diaponeurosporen-4-al and achieves substrate specificity.

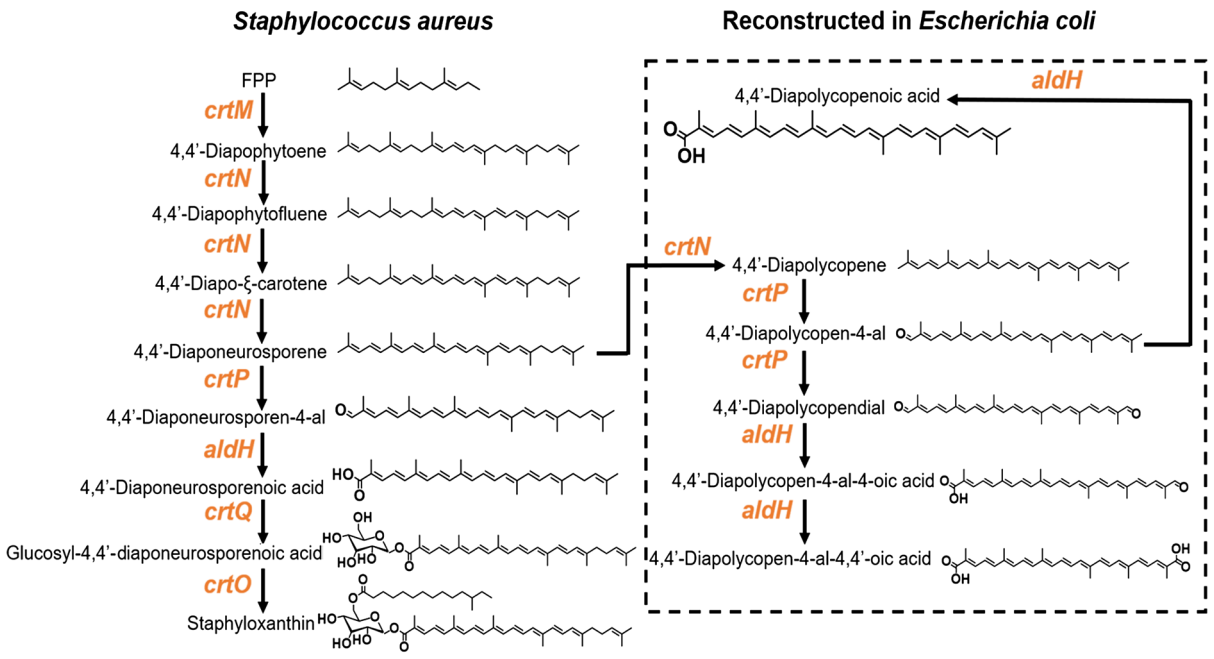

Figure 1 | *Staphyloxanthin biosynthetic pathway in S. aureus and reconstructed biosynthetic pathway in E. coli. Structures of carotenoids produced in recombinant E. coli host, but not in S. aureus, are shown in the dashed box.*

DOI: 10.31635/ccschem.020.202000219
Citation: *CCS Chem.* **2020**, 2, 946–954
Citation denotes calendar and volume year of first online publication.
Issue Assignment: Volume 2 (2020), Issue 5

Herein, we report the crystal structures of apo- and holo-forms of *Sa*AldH. Unexpectedly, the bacterial ALDH family protein contains a unique C-terminal α-helix, which resembles a membrane-bound human fatty aldehyde dehydrogenase (FALDH). Particularly, the C-helix adopts different conformations in apo- and holo-*Sa*AldH to control the substrate tunnel access. *In vitro* enzymatic assay, H_2O_2 sensitivity, and macrophage killing assays reveal key residues essential for *Sa*AldH catalytic turnover. Our studies provide the first structural basis for the substrate recognition and catalysis of *Sa*AldH in the staphyloxanthin biosynthetic pathway.

Experimental Methods

Detailed experimental methods are available in the Supporting Information.

Results and Discussion

Apo-*Sa*AldH forms a dimer with a unique C-terminal helix

*Sa*AldH cDNA was cloned into a pET47b vector and expressed as a His_6-fusion protein in *E. coli*(Supporting Information Table S1). To obtain a stable protein sample, the dehydrogenase active site C244 of *Sa*AldH was mutated to serine. The fusion protein was purified by a Ni affinity column and subsequently digested by PreScission protease to remove the His_6-fusion. *Sa*AldH^{C244S} was eluted from Tricorn Superdex 200 column at 13.3 mL with a calculated molecular weight of 100 kDa, corresponding to a dimeric form (calculated molecular weight of monomeric *Sa*AldH is 51.7 kDa). Purified apo-form *Sa*AldH^{C244S} was assayed for crystallization and yielded three-dimensional crystals for X-ray diffraction experiments (see Supporting Information Table S2).

The crystals of apo-*Sa*AldH^{C244S} belong to the $P22_12_1$ space group and diffract to a resolution of 1.8 Å. Initial phases were obtained by molecular replacement using human FALDH (PDBID: 4QGK) as a search model. The final structure model contains only one chain of *Sa*AldH in one asymmetric unit and was refined to a R_{work} of 21.3% and R_{free} of 23.9%. Apo-*Sa*AldH structure adopts the typical aldehyde dehydrogenase fold with a NAD(P)$^+$-binding domain (residues 2–84 and 106–211), a catalytic domain (residues 212–424), and a bridging domain connecting the two subunits of the dimer (residues 85–105 and 425–446) (Figure 2a).[23] Clear but discontinuous electron density is found at the NAD(P)$^+$-binding domain, which is likely due to the low occupancy of the NAD(P)$^+$ cofactor. In the *Sa*AldH structure, the NAD(P)$^+$-binding site consists of residues I111, F114, N115, E141, T143, V169, T173, I177, G188, V191, I195, V196, F234, and F338. Sequence alignments show that each residue is similar among the ALDH homologues, indicative of a highly conserved NAD(P)$^+$-binding site in the ALDH superfamily (Supporting Information Figure S1).

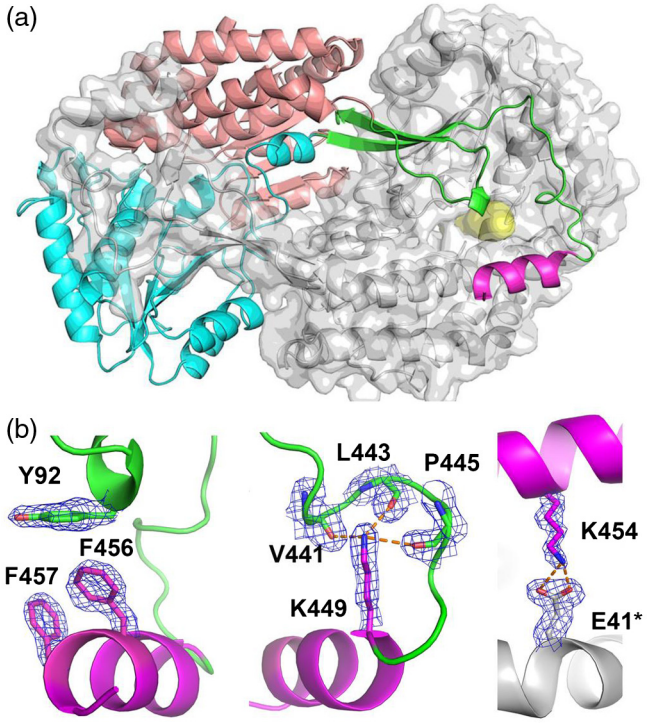

Figure 2 | *Structure of* Sa*AldH. (a)* Sa*AldH is a symmetrical homodimer with a large dimerization interface. One subunit is shown as a cartoon model, the catalytic domain (cyan residues 212–424), NAD(P)$^+$-binding domain (wheat residues 2–84 and 106–211), bridging domain (green residues 85–105 and 425–446), and C-terminal helix (magenta residues 447–458) are shown. The other subunit is shown as a surface model in gray. The substrate tunnel is shown in yellow. (b) The C-terminal helix is stabilized by both polar and hydrophobic interactions. The T-shaped π–π stacking interactions among residues F456, F457, and Y92, hydrogen bonding between K449 and residues 440–445, and the salt bridge between K454 and E41 from adjacent subunits (E41*) are shown in the stick model. All residues visible in electron density are shown. $2F_o$–F_c density at 1σ is shown as mesh.*

Opposite the NAD(P)$^+$-binding site is the substrate binding tunnel, which is built up by residues A61, T62, I66, Y116, Q119, T243, S244, V245, M395, L397, A398, and F404 from one subunit and Y92, L93, H442, I453, F456, and F457 from the adjacent subunit of the dimer. Intriguingly, distinct from the highly conserved NAD(P)$^+$-binding site, the residues built up from the substrate tunnel are highly variable in different ALDH homologues (Supporting Information Figure S1), which is probably attributable to different substrate specificity.

Unexpectedly, the C-terminal residues 449–459 form a short α-helix and are located near the substrate tunnel

DOI: 10.31635/ccschem.020.202000219
Citation: *CCS Chem.* **2020**, 2, 946–954
Citation denotes calendar and volume year of first online publication.
Issue Assignment: Volume 2 (2020), Issue 5

entrance, which resembles a "gatekeeper" helix identified in the human membrane-associated FALDH.[20] The helix is stabilized by both polar and hydrophobic interactions, such as a hydrogen-bonded network between the K449 side chain and backbone atoms in a loop region consisting of residues 440–445 and a salt bridge between K454 and E41 from the adjacent subunit. Particularly, side chains of F456 and F457 point to the substrate tunnel and form T-shaped π–π stacking interactions with Y92 (Figure 2b). Previous studies have demonstrated that the FALDH C-helix induces a 93° kink in the direction of the substrate cavity.[20] Intriguingly, although *Sa*AldH C-helix also lies close to the access of the substrate tunnel, no such kink was observed for the *Sa*AldH substrate cavity as calculated using the MOLE toolkit (Supporting Information Figure S2).[24] Structure superimposition of *Sa*AldH and FALDH reveals that the two structures are quite similar with a backbone r.m.s.d value of 0.811 Å. However, the orientations of the C-helices are different. *Sa*AldH C-helix forms an 18.2° angle with the corresponding C-helix in FALDH (Figure 3a). Moreover, side chains of W450, F454, and L438 in FALDH C-helix point to the entry and block the access to the cavity, which prevents the direct entry of the substrate. In contrast, the *Sa*AldH C-helix does not block the entry, so the substrate can enter the tunnel (Figures 3b and 3c).

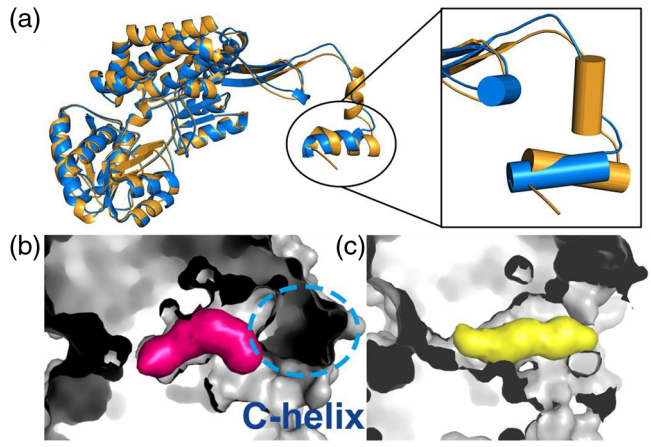

Figure 3 | *The C-terminal helices of human FALDH and* Sa*ALDH adopt different conformations. (a) Structure superimposition between human FALDH (orange) and apo-*Sa*AldH (marine). The two C-helices adopt different orientations. (b and c) Cross-section through the active sites of FALDH and apo-*Sa*AldH. The substrate tunnels are characterized using the MOLE toolkit for PyMOL. In FALDH, the C-helix (highlighted in dashed circle) creates a kink in the tunnel (shown in magenta). While the linear arrangement of the substrate tunnel of apo-*Sa*AldH (shown in yellow) is not restricted by the C-helix.*

The substrate tunnel in holo-*Sa*AldH adopts a "closed" conformation

To understand, in detail, how the substrate is bound in *Sa*AldH, we obtained the crystal structure of substrate-bound (holo) *Sa*AldH. In a previous study, it was reported that reconstitution of *crtM*, *crtN,* and *crtP* genes in *E. coli* led to the accumulation of *Sa*AldH substrate 4,4'-diaponeuros-poren-4-al.[16] We envision that coexpression of CrtM, CrtN, CrtP, and an inactive *Sa*AldH^{C244S} mutant can result in a substrate-bound state of *Sa*AldH. As expected, the purified *Sa*AldH^{C244S} mutant coexpressed with CrtM/N/P gave a reddish color. Mass spectrometric analysis of a lipid extract of the purified *Sa*AldH^{C244S} sample indicated the presence of 4,4'-diapoly-copen-4-al, a fully unsaturated analogue of 4,4'-diaponeuros-poren-4-al (Figure 1 and Supporting Information Figure S3). The substrate analogue is usually found in *E. coli* artificial synthetic systems as described previously.[16] Holo-*Sa*AldH crystals with reddish-brown color were grown by a vapor diffusion method, and mass spectrometric analysis confirmed the presence of 4,4'-diapolycopen-4-al substrate in the protein crystals (Supporting Information Figure S3). The crystals belong to the space group *I*422 and are diffracted to a resolution of 2.6 Å. Analysis of the holo-*Sa*AldH structure reveals only a triangular-shaped electron density peak at the catalytic site with an approximate distance of 2.7 Å away from the catalytic residue C244 (mutated to S244). Unexpectedly, no electron density was observed in the substrate tunnel, although mass spectra data confirmed the presence of substrate, which is probably attributed to the long and potentially flexible chain of the substrate.

Intriguingly, a significant orientation change of the C-helix was observed in holo-*Sa*AldH by superimposing the apo- and holo-*Sa*AldH structures. Holo-*Sa*AldH C-helix has a 10.6° swing-in toward the tunnel entrance compared to the apo-form (Figure 4a). This C-helix swing-in results in substantial movement of F456 and F457 side chains, which insert into the substrate tunnel. Notably, no electron density was observed for Y92 side chain in holo-*Sa*AldH. All these data suggest the disruption of the T-shaped π–π stacking interactions among F456, F456, and Y92 found in apo-*Sa*AldH. Furthermore, the residues V441 and H442 in a preceding loop also move toward the substrate tunnel in holo-*Sa*AldH (Figure 4b). It is worth noting that the swing-in C-helix in holo-*Sa*AldH blocks the entrance of the substrate tunnel (Figures 4c and 4d). Moreover, this conformational change also induces a 52.6° kink in the direction of the substrate tunnel (Supporting Information Figure S2). This configuration suggests that this unique C-helix might function as an important "gate" for the substrate tunnel. In the apo-state, the C-helix adopts an "open" conformation and allows enzyme substrate entry. Once the specific substrate obtains access into the substrate tunnel, the C-helix undergoes a conformational change

DOI: 10.31635/ccschem.020.202000219
Citation: *CCS Chem.* **2020**, 2, 946–954
Citation denotes calendar and volume year of first online publication.
Issue Assignment: Volume 2 (2020), Issue 5

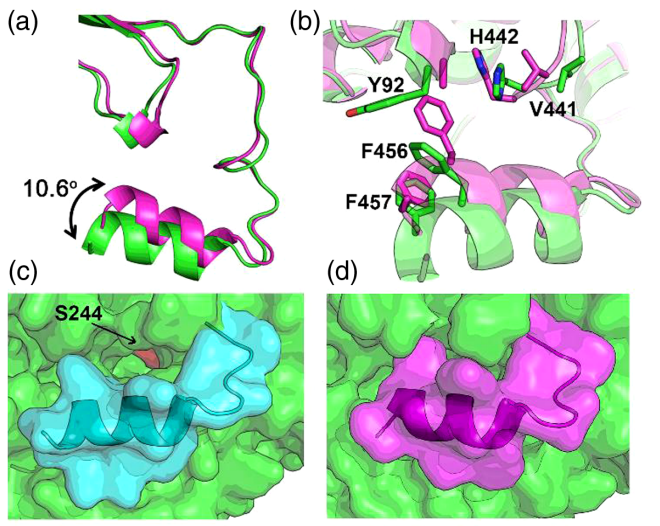

Figure 4 | *The substrate tunnels in S. aureus apo- and holo-AldH adopt "open" and "closed" conformations, respectively. (a) Structural superimposition of S. aureus apo- (green) and holo-AldH (magenta). The "swing-in" movement of C-helix is shown in the cartoon model. (b) The side chains of residues Y92, V441, H442, F456, and F457 are shown as stick models in apo- (green) and holo-AldH (magenta). (c and d) The "open" and "closed" conformations of the S. aureus AldH substrate tunnel. The structures are shown in the surface model. The C-helices in apo- and holo-AldH are highlighted in cyan and magenta, respectively. The catalytic residue C244 (mutated to S244) is colored in red.*

to block the tunnel entrance and lock the substrate, exhibiting a "closed" conformation.

A substrate-bound structure model of *Sa*AldH

The "open" to "closed" conformational change of *Sa*AldH C-helix is likely attributed to substrate binding. To further elucidate the substrate binding pattern, the binding of 4,4'-diapolycopen-4-al to holo-*Sa*AldH was modeled using the molecular docking program, Autodock4.[25] The grid box was set to cover the substrate tunnel calculated by the MOLE toolkit. The calculated structure model with the lowest energy was selected to represent the substrate–*Sa*AldH complex (Supporting Information). As shown in Figure 5a, the 4,4'-diapolycopen-4-al molecule can fit well into the substrate tunnel. The aldehyde group is close to the catalytic residue C244 (mutated to S244) with a distance of 3.7 Å. The kink of the substrate tunnel induces a distortion of the substrate molecule 4,4'-diapolycopen-4-al. The substrate forms intensive hydrophobic interactions with the residues located in the substrate tunnel, including A61, I66, Y116, P90, A398, P400, I453, F456, and F457 from the adjacent subunit (Figure 5a). In particular, Y116 forms a π–σ interaction with the 2-methyl group, while the F456 at the C-helix forms a parallel-displaced π–π stacking with F457 and hydrophobic interactions with the two terminal methyl groups of the substrate. This structural model indicates that the C-helix is likely to participate in substrate recognition during enzymatic catalysis.

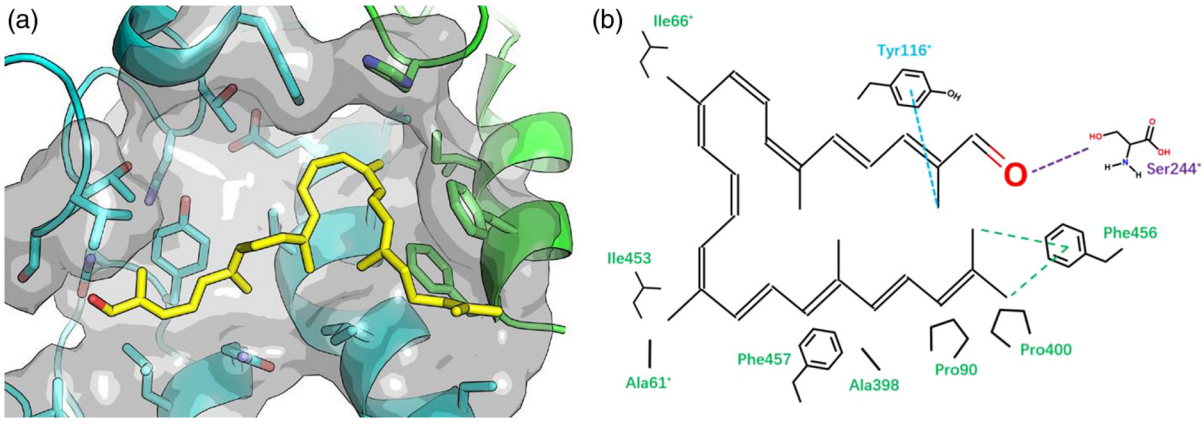

Figure 5 | *Structure model of S. aureus holo-AldH binding to the substrate. (a) Cross-section through the substrate tunnel of holo-AldH (cyan). The C-helix is highlighted in green. The 4,4'-diapolycopen-4-al substrate (yellow) and the residue side chains lining the substrate tunnel are shown in the stick model. The distance between the aldehyde group and the catalytic residue (S244) is 3.7 Å. (b) Analysis of the interactions between 4,4'-diapolycopen-4-al and AldH residues in the substrate tunnel. The residues involved in hydrophobic interactions are colored in green. The σ–π interaction between the substrate methyl group and Y116 side chain is colored in cyan. The interaction between the substrate aldehyde group and catalytic residue (S244) side chain is colored in purple.*

DOI: 10.31635/ccschem.020.202000219
Citation: *CCS Chem.* **2020**, 2, 946–954
Citation denotes calendar and volume year of first online publication.
Issue Assignment: Volume 2 (2020), Issue 5

Critical residues for *Sa*AldH enzymatic activity

The structures of apo- and holo-forms of *Sa*AldH demonstrate that the unique C-helix might exert an important role in controlling the access of the substrate tunnel and recognizing a specific substrate. Several residues were identified as conformation stabilizers of the C-helix. For example, the K449 residue is engaged in a hydrogen bond network with the backbone oxygen atoms of V441, L443, and P445 in apo-*Sa*AldH. Mutagenesis of the corresponding residue in human FALDH (K447 in FALDH) reduced the enzyme catalytic capacity for long-chain fatty aldehyde.[20] The F456, F457, and Y92 form T-shaped π–π stacking to stabilize the C-terminus of the helix in apo-*Sa*AldH. Furthermore, the F456 and F457 are also engaged in substrate recognition in the holo-*Sa*AldH structure model. We envision that conformational disturbance of the C-helix interferes with *Sa*AldH enzymatic activity. To test our hypothesis, we mutated residues K449, Y92, F456, and F457 to alanine and compared their activities using either benzaldehyde or 4,4'-diapolycopen-4-al as substrates.

When benzaldehyde was used as a substrate, the *Sa*AldH^{K449E} mutant showed similar enzymatic activity

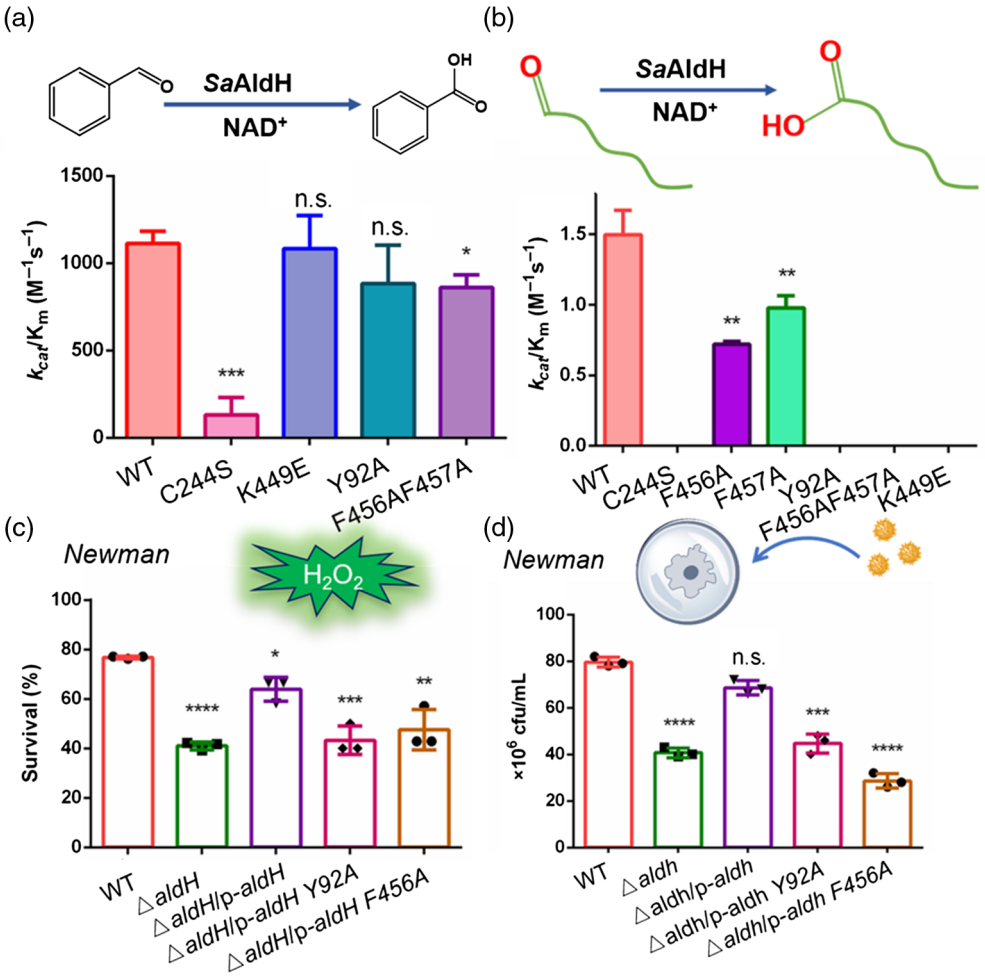

Figure 6 | *The C-helix residues are important for S. aureus AldH activity. (a) Comparison of the catalytic capacity (k_{cat}/K_m) of wide-type (WT) S. aureus AldH and different mutants to metabolize benzaldehyde. The K449E and Y92A mutants have the same catalytic capacities as WT-AldH, while the F456A/F457A double-mutant only causes 15% decrease in catalytic efficiency. (b) Comparison of the dehydrogenase activity of WT-AldH and mutants toward 4,4'-diapolycopen-4-al. F456 and F457 single mutants lead to 50% and 40% decreases on catalytic efficiency, respectively. K449E, Y92A, and F456A/F457 mutants have no detectable activities. Resistance capability comparison of S. aureus Newman and different mutants against H_2O_2 (c) and macrophage phagocytosis (d)* aldH *gene knockout significantly attenuates the resistance capability of S. aureus against H_2O_2 and macrophage phagocytosis. Complementation of* aldH *Y92A and F456A mutant genes cannot restore the capability. Each experiment was performed in triplicates. The data are shown in mean ± SD. *p < 0.05, **p < 0.01, ***p < 0.001, ****p < 0.0001, n. s. not significant.*

DOI: 10.31635/ccschem.020.202000219
Citation: *CCS Chem.* **2020**, 2, 946–954
Citation denotes calendar and volume year of first online publication.
Issue Assignment: Volume 2 (2020), Issue 5

compared to that of wild-type (WT) *Sa*AldH. The *Sa*AldH^{Y92A} and the double-mutant *Sa*AldH$^{F456A/F457A}$ retain approximately 80% activity, as compared to WT-*Sa*AldH, indicating that these mutations do not significantly compromise *Sa*AldH catalytic capacity for benzaldehyde (Figure 6a and Supporting Information Table S3). Remarkably, however, when the long-chain 4,4'-diapolycopen-4-al was used as a substrate, the mutants *Sa*AldH^{K449E} and *Sa*AldH^{Y92A} have no detectable enzyme activities. Single mutations of F456A and F457A resulted in substantially lower enzyme activities with 48% and 66% WT-*Sa*AldH activity being retained, respectively, while the double-mutant *Sa*AldH$^{F456A/F457A}$ completely lost the catalytic capacity for the 4,4'-diapolycopen-4-al substrate (Figure 6b). Consistent with the enzymatic assay data *in vitro*, coexpression of these *Sa*AldH mutants with CrtM, CrtN, and CrtP in *E. coli* also resulted in significant accumulation of 4,4'-diapolycopen-4-al, which could not be further metabolized (Supporting Information Figure S4). This indicates that the residues stabilizing the C-helix conformation are not directly involved in enzyme catalysis but are essential for recognition and efficient metabolism of 4,4'-diapolycopen-4-al substrate.

It has been reported that staphyloxanthin functions as an antioxidant to protect *S. aureus* against exogenous reactive oxidative species (ROS) as well as host innate immunity.[7,8] Blocking the staphyloxanthin biosynthesis pathway can lead to enhanced susceptibility of *S. aureus* to oxidative stress or whole blood killing.[11,12] Therefore, we further investigated whether these *Sa*AldH mutations affected *S. aureus* sensitivity to oxidative stress and macrophage killing. An *aldH* gene-deleted mutant of *S. aureus* Newman strain (*S. aureus* Δ*aldH*) was constructed using the recently reported pCasSA system,[26] and *S. aureus* Δ*aldH* mutant was complemented with WT or mutated *aldH* genes using the pCL55 plasmid as previously described (see Supporting Information).[27] When treated with 10 mM H_2O_2 for 45 min, the survival rate of *S. aureus* Δ*aldH* mutant was about 42%, only half of that for WT *S. aureus*, implicating that *Sa*AldH is essential for *S. aureus* to survive under H_2O_2 oxidative stress (Figure 6c). Complementation of WT-*aldH* genes can substantially enhance Δ*aldH* mutant's tolerance to H_2O_2. In contrast, *aldH* genes with Y92A or F456A mutants were unable to increase the survival rate of the Δ*aldH* mutant. Consistent with H_2O_2 sensitivity assays, macrophage killing experiments also demonstrate that Y92A and F456A mutants significantly decrease *S. aureus* viability during macrophage phagocytosis, indicating the essential role of staphyloxanthin to protect *S. aureus* from macrophage-based human innate immunity (Figure 6d).

Conclusions

The structures of *S. aureus* AldH reveal a novel C-terminal α-helix in a bacterial aldehyde dehydrogenase, which controls access to the substrate cavity and exerts a critical role in recognizing a specific polyunsaturated aldehyde substrate. Although *Sa*AldH is a bacterial aldehyde dehydrogenase, sequence alignment demonstrates that *Sa*AldH has a 45.4% sequence identity with human membrane-bound FALDH. In contrast, it only has 28.3% and 30.4% identity with two other ALDH homologues in *S. aureus* Newman strains (UniProt accession ID: A0A0H3K9N0 and A0A0H3K677), respectively (Supporting Information Figure S1).

*Sa*AldH contains a hydrophobic C-helix as identified in human FALDH, whereas no such C-terminal sequence is found in two other *S. aureus* ALDH homologues, indicating that this C-helix is unique for staphyloxanthin biosynthesis. Site-directed mutagenesis of *Sa*AldH that perturbsC-helix conformation significantly attenuate the catalytic capacity of *Sa*AldH toward 4,4'-diapolycopen-4-al, but not benzaldehyde, implying that the C-helix is important for long-chain aldehyde substrate recognition. Indeed, our structural model of the holo-*Sa*AldH complex with 4,4'-diapolycopen-4-al reveals intensive hydrophobic contact between the substrate and residues on C-helix. Moreover, our structural analysis demonstrates that the C-helix can adopt two distinct conformations: an "open" conformation in apo-*Sa*AldH and a "closed" conformation in holo-*Sa*AldH. Although we did not observe the substrate electron density in the holo-*Sa*AldH structure, the plausible mechanism is that the long-chain aldehyde can enter the "open" substrate cavity of apo-*Sa*AldH. Subsequently, the hydrophobic interactions between the substrate tail and C-helix cause the "swing-in" movement of the C-helix, which caps the entry of the substrate tunnel and prevents the release of the substrate before enzymatic catalysis. Previous studies have demonstrated that the release of the ALDH product is coupled with the NADH cofactor.[28] Therefore, the release of the NADPH cofactor from *Sa*AldH after enzymatic catalysis might cause a conformational change at the C-helix, which finally leads to product release from the substrate tunnel.

It is worth noting that most of the amino acids lining the substrate tunnel are hydrophobic (Supporting Information Figure S1). Therefore, the side chains of these amino acids may participate in substrate selection by providing a hydrophobic cavity to accommodate the 4,4'-diapolycopen-4-al substrate, which contains a hydrophobic tail. Furthermore, analysis of the substrate tunnels indicates that the length of *Sa*AldH substrate tunnel is around 26 Å. Therefore, it could allow a longer substrate than human FALDH, which has a substrate tunnel length of 19 Å (Supporting Information Figure S2). Together, these factors are likely to contribute to specific substrate recognition by *Sa*AldH.

Previous studies of mammalian class 3 ALDHs suggest that the C-helix may be a distinct feature of membrane-associated ALDH enzymes.[20] Human FALDH has an extended transmembrane domain, while human

DOI: 10.31635/ccschem.020.202000219
Citation: *CCS Chem.* **2020**, 2, 946–954
Citation denotes calendar and volume year of first online publication.
Issue Assignment: Volume 2 (2020), Issue 5

ALDH3B1 is anchored to plasma membrane via C-terminal palmitoylation or prenylation.[29] In both cases, the enzyme substrate tunnel entries and C-helices are oriented toward the lipid layer to facilitate their specificity toward fatty aldehyde resulted from lipid-derived oxidative stress.[30] Although *Sa*AldH contains a similar C-helix, it is unknown whether *Sa*AldH is a membrane-associated enzyme. Intriguingly, the crystal structure of *S. aureus* AldH revealed that, together with K447, K449, K451, and K458 on the C-helix, positively charged residues R26, K27, K35, K38, K69, K72, R75, K76, K79, K83, K85, K97, K101, and K102 constitute a basic amino-acid cluster providing positive electrostatic surface potential (Supporting Information Figure S5). Previous studies have demonstrated that the final biosynthetic product staphyloxanthin is embedded in the micro-domain of the *S. aureus* membrane to maintain bacterial membrane integrity.[9] Intriguingly, the two downstream enzymes in the staphyloxanthin biosynthetic pathway, CrtQ and CrtO, were identified to be membrane-associated enzymes.[31] It is reasonable to speculate that this positively charged surface might facilitate *Sa*AldH to associate with the bacterial membrane so that the hydrophobic product from *Sa*AldH can be efficiently transferred to the following biosynthetic enzymes. Therefore, the subcellular location of *Sa*AldH is warranted for further investigation.

Supporting Information

Supporting Information is available.

Conflict of Interest Statement

There is no conflict of interest to report.

Funding Information

This work was supported by the National Natural Science Foundation of China (21671203 and 21877131), RGC of Hong Kong (17305415 and 17333616), the Ministry of Education of China (IRT-17R111), and the Fundamental Research Funds for the Central Universities.

Acknowledgments

The authors thank Qi Huang, Yu Guo, and Yanxuan Xie for their helpful discussions regarding the experimental design. The authors are also grateful to Xia Li for her help with the TCL-MS data collection.

References

1. Lowy, F. D. Staphylococcus aureus Infections. *New Engl. J. Med.* **1998**, *339*, 520–532.
2. Klevens, R. M.; Morrison, M. A.; Nadle, J.; Petit, S.; Gershman, K.; Ray, S.; Harrison, L. H.; Lynfield, R.; Dumyati, G.; Townes, J. M.; Craig, A. S.; Zell, E. R.; Fosheim, G. E.; McDougal, L. K.; Carey, R. B.; Fridkin, S. K.; Surveillance Investigators, A. Invasive methicillin-resistant Staphylococcus aureus infections in the United States. *JAMA.* **2007**, 298, 1763–1771.
3. Kong, C.; Neoh, H. M.; Nathan, S. Targeting Staphylococcus aureus Toxins: A Potential form of Anti-Virulence Therapy. *Toxins.* **2016**, 8, 72.
4. Clatworthy, A. E.; Pierson, E.; Hung, D. T. Targeting Virulence: A New Paradigm for Antimicrobial Therapy. *Nat. Chem. Biol.* **2007**, *3*, 541–548.
5. Rasko, D. A.; Sperandio, V. Anti-Virulence Strategies to Combat Bacteria-Mediated Disease. *Nat. Rev. Drug Discov.* **2010**, *9*, 117–128.
6. Becker, K.; Skov , R.; von Eiff , C.. **2015**. Staphylococcus, Micrococcus, and Other Catalase-Positive Cocci.Jorgensen, J.; Pfaller, M. A.; Carroll, K.; Funke, G.; Landry, M.; Richter, S.; Warnock, D. (Eds.), Manual of Clinical Microbiology, Eleventh Edition.. ASM Press, Washington, DC. p. 354–382.
7. Clauditz, A.; Resch, A.; Wieland, K.-P.; Peschel, A.; Götz, F. Staphyloxanthin Plays a Role in the Fitness of Staphylococcus aureus and its Ability to Cope with Oxidative Stress. *Infect. Immun.* **2006**, *74*, 4950–4953.
8. Liu, G. Y.; Essex, A.; Buchanan, J. T.; Datta, V.; Hoffman, H. M.; Bastian, J. F.; Fierer, J.; Nizet, V. Staphylococcus aureus Golden Pigment Impairs Neutrophil Killing and Promotes Virulence through its Antioxidant Activity. *J. Exp. Med.* **2005**, *202*, 209–215.
9. García-Fernández, E.; Koch, G.; Wagner, R. M.; Fekete, A.; Stengel, S. T.; Schneider, J.; Mielich-Süss, B.; Geibel, S.; Markert, S. M.; Stigloher, C.; Lopez, D. Membrane Microdomain Disassembly Inhibits MRSA Antibiotic Resistance. *Cell.* **2017**, 171, 1354.
10. Mishra, N. N.; Liu, G. Y.; Yeaman, M. R.; Nast, C. C.; Proctor, R. A.; McKinnell, J.; Bayer, A. S. Carotenoid-Related Alteration of Cell Membrane Fluidity Impacts Staphylococcus aureus Susceptibility to Host Defense Peptides. *Antimicrob. Agents Chemother.* **2011**, 55, 526–531.
11. Liu, C.-I.; Liu, G. Y.; Song, Y.; Yin, F.; Hensler, M. E.; Jeng, W.-Y.; Nizet, V.; Wang, A.; Oldfield, E. A Cholesterol Biosynthesis Inhibitor Blocks Staphylococcus aureus Virulence. *Science.* **2008**, 319, 1391–1394.
12. Chen, F.; Di, H.; Wang, Y.; Cao, Q.; Xu, B.; Zhang, X.; Yang, N.; Liu, G.; Yang, C.-G.; Xu, Y.; Jiang, H.; Lian, F.; Zhang, N.; Li, J.; Lan, L. Small-Molecule Targeting of a Diapophytoene Desaturase Inhibits S. aureus Virulence. *Nat. Chem. Biol.* **2016**, *12*, 174–179.
13. Gao, P.; Davies, J.; Kao, R. Dehydrosqualene Desaturase as a Novel Target for Anti-Virulence Therapy Against Staphylococcus aureus. *mBio.* **2017**, 8, 17.
14. Wieland, B.; Feil, C.; Gloria-Maercker, E.; Thumm, G.; Lechner, M.; Bravo, J. M.; Poralla, K.; Götz, F. Genetic and Biochemical Analyses of the Biosynthesis of the Yellow Carotenoid 4,4′-Diaponeurosporene of Staphylococcus aureus. *J. Bacteriol.* **1994**, *176*, 7719–7726.
15. Pelz, A.; Wieland, K.-P.; Putzbach, K.; Hentschel, P.; Albert, K.; Götz, F. Structure and Biosynthesis of

Staphyloxanthin from Staphylococcus aureus. *J. Biol. Chem.* **2005**, *280*, 32493–32498.
16. Kim, S.; Lee, P. Functional Expression and Extension of Staphylococcal Staphyloxanthin Biosynthetic Pathway in Escherichia coli. *J. Biol. Chem.* **2012**, *287*, 21575–21583.
17. Marchitti, S. A.; Brocker, C.; Stagos, D.; Vasiliou, V. Non-P450 Aldehyde Oxidizing Enzymes: The Aldehyde Dehydrogenase Superfamily. *Expert Opin. Drug Metab. Toxicol.* **2008**, *4*, 697–720.
18. Moore, S. A.; Baker, H. M.; Blythe, T. J.; Kitson, K. E.; Kitson, T. M.; Baker, E. N. Sheep Liver Cytosolic Aldehyde Dehydrogenase: The Structure Reveals the Basis for the Retinal Specificity of Class 1 Aldehyde Dehydrogenases. *Structure.* **1998**, 6, 1541–1551.
19. Steinmetz, C. G.; Xie, P.; Weiner, H.; Hurley, T. D. Structure of Mitochondrial Aldehyde Dehydrogenase: The Genetic Component of Ethanol Aversion. *Structure.* **1997**, 5, 701–711.
20. Keller, M. A.; Zander, U.; Fuchs, J. E.; Kreutz, C.; Watschinger, K.; Mueller, T.; Golderer, G.; Liedl, K. R.; Ralser, M.; Krautler, B.; Werner, E. R.; Marquez, J. A. A Gatekeeper Helix Determines the Substrate Specificity of Sjogren–Larsson Syndrome Enzyme Fatty Aldehyde Dehydrogenase. *Nat. Commun.* **2014**, 5, 4439.
21. Kitson, K. E.; Blythe, T. J. The Hunt for a Retinal-Specific Aldehyde Dehydrogenase in Sheep Liver. *Adv. Exp. Med. Biol.* **1999**, *463*, 213–221.
22. Klyosov, A. A.; Rashkovetsky, L. G.; Tahir, M. K.; Keung, W. M. Possible Role of Liver Cytosolic and Mitochondrial Aldehyde Dehydrogenases in Acetaldehyde Metabolism. *Biochemistry.* **1996**, 35, 4445–4456.
23. Liu, Z. J.; Sun, Y. J.; Rose, J.; Chung, Y. J.; Hsiao, C. D.; Chang, W. R.; Kuo, I.; Perozich, J.; Lindahl, R.; Hempel, J.; Wang, B. C. The First Structure of An Aldehyde Dehydrogenase Reveals Novel Interactions Between NAD and the Rossmann Fold. *Nat. Struct. Mol. Biol.* **1997**, *4*, 317–326.
24. Sehnal, D.; Svobodova Varekova, R.; Berka, K.; Pravda, L.; Navratilova, V.; Banas, P.; Ionescu, C. M.; Otyepka, M.; Koca, J. MOLE 2.0: Advanced Approach for Analysis of Biomacromolecular Channels. *J. Cheminform.* **2013**, *5*, 39.
25. Morris, G. M.; Huey, R.; Lindstrom, W.; Sanner, M. F.; Belew, R. K.; Goodsell, D. S.; Olson, A. J. AutoDock4 and AutoDockTools4: Automated Docking with Selective Receptor Flexibility. *J. Comput. Chem.* **2009**, *30*, 2785–2791.
26. Chen, W.; Zhang, Y.; Yeo, W.-S.; Bae, T.; Ji, Q. Rapid and Efficient Genome Editing in Staphylococcus aureus by Using an Engineered CRISPR/Cas9 System. *J. Am. Chem. Soc.* **2017**, *139*, 3790–3795.
27. Lee, C. Y.; Buranen, S. L.; Ye, Z. H. Construction of Single-Copy Integration Vectors for Staphylococcus aureus.*Gene.* **1991**, *103*, 101–105.
28. Moretti, A.; Li, J.; Donini, S.; Sobol, R. W.; Rizzi, M.; Garavaglia, S. Crystal Structure of Human Aldehyde Dehydrogenase 1A3 Complexed with NAD(+) and Retinoic Acid. *Sci. Rep.* **2016**, 6, 35710.
29. Kitamura, T.; Naganuma, T.; Abe, K.; Nakahara, K.; Ohno, Y.; Kihara, A. Substrate Specificity, Plasma Membrane Localization, and Lipid Modification of the Aldehyde Dehydrogenase ALDH3B1. *Biochim. Biophys. Acta.* **2013**, *1831*, 1395–1401.
30. Marchitti, S. A.; Brocker, C.; Orlicky, D. J.; Vasiliou, V. Molecular Characterization, Expression Analysis, and Role of ALDH3B1 in the Cellular Protection Against Oxidative Stress. *Free Radic. Biol. Med.* **2010**, *49*, 1432–1443.
31. Zhang, L.; Selao, T. T.; Selstam, E.; Norling, B. Subcellular Localization of Carotenoid Biosynthesis in Synechocystis sp. PCC 6803. *PLoS One.* **2015**, 10, e0130904.

DOI: 10.31635/ccschem.020.202000219
Citation: *CCS Chem.* **2020**, 2, 946–954
Citation denotes calendar and volume year of first online publication.
Issue Assignment: Volume 2 (2020), Issue 5